Published in final edited form as:

Science. 2019 September 13; 365(6458): 1138–1143. doi:10.1126/science.aax4423.

Synthesis of a copper-supported triplet nitrene complex pertinent to copper-catalyzed amination

Kurtis M. Carsch[1], **Ida M. DiMucci**[2], **Diana A. Iovan**[1], **Alex Li**[1], **Shao-Liang Zheng**[1], **Charles J. Titus**[3], **Sang Jun Lee**[4], **Kent D. Irwin**[3,5], **Dennis Nordlund**[4], **Kyle M. Lancaster**[2,*], **Theodore A. Betley**[1,*]

[1]Department of Chemistry and Chemical Biology, Harvard University, Cambridge, MA, USA.

[2]Department of Chemistry and Chemical Biology, Cornell University, Ithaca, NY, USA.

[3]Department of Physics, Stanford University, Stanford, CA, USA.

[4]Stanford Synchrotron Radiation Lightsource, SLAC National Accelerator Laboratory, Menlo Park, CA, USA.

[5]SLAC National Accelerator Laboratory, Menlo Park, CA, USA.

Abstract

Terminal copper-nitrenoid complexes have inspired interest in their fundamental bonding structures as well as their putative intermediacy in catalytic nitrene-transfer reactions. Here, we report that aryl azides react with a copper(I) dinitrogen complex bearing a sterically encumbered dipyrrin ligand to produce terminal copper nitrene complexes with near-linear, short copper–nitrenoid bonds [1.745(2) to 1.759(2) angstroms]. X-ray absorption spectroscopy and quantum chemistry calculations reveal a predominantly triplet nitrene adduct bound to copper(I), as opposed to copper(II) or copper(III) assignments, indicating the absence of a copper–nitrogen multiple-bond character. Employing electron-deficient aryl azides renders the copper nitrene species competent for alkane amination and alkene aziridination, lending further credence to the intermediacy of this species in proposed nitrene-transfer mechanisms.

Copper-catalyzed nitrene delivery is a powerful methodology for the construction of C–N bonds (1–3). Advances since the seminal work of Kwart and Kahn (4) on copper-catalyzed

[*]**Corresponding author.** betley@chemistry.harvard.edu (T.A.B.); kml236@cornell.edu (K.M.L.).

Author contributions: K.M.C. and T.A.B. conceived the experimental design, executed syntheses, conducted data analysis, and assessed nitrene group transfer. I.M.D. and K.M.L. performed XANES measurements and conducted both the data interpretation and computational analysis. D.A.I. performed initial reactivity studies. A.L. assisted K.M.C. in substrate synthesis. C.J.T., S.J.L., K.D.I., and D.N. were responsible for data processing of Cu $L_{2,3}$-edge and N K-edge data. S.-L.Z. assisted K.M.C. in crystallographic refinement. All authors contributed to the construction of the manuscript.

Competing interests: The authors declare no competing interests.

Data and materials availability: Supporting spectra are included in the supplementary materials. Crystallographic data can be obtained free of charge from the Cambridge Crystallographic Data Centre (www.ccdc.cam.ac.uk/data_request/cif): **1** (1901023), **2** (1901025), **3** (1901026), **4** (1901027), **5** (1901028), **6** (1901029), **7** (1901033), **8** (1901030), **9** (1901032), and **10** (1901031).

SUPPLEMENTARY MATERIALS

science.sciencemag.org/content/365/6458/1138/suppl/DC1 Materials and Methods
Supplementary Text Figs. S1 to S93 Tables S1 to S12
Cartesian Coordinates (Computations) References (*64–113*)
CheckCIF Reports

C–N bond formation in the past five decades include alkane (5–8) and arene (9, 10) amination, asymmetric alkene aziridination (11, 12), and natural product syntheses (13–16). In the foregoing transformations, terminal copper-nitrenoid complexes have been invoked as critical intermediates; nonetheless, the spectroscopic detection and direct isolation of an authentic terminal copper-nitrenoid complex as proposed (6–10, 17–22) remains elusive (23, 24). The presence of Cu(NR) functionalities can be inferred from kinetic analysis of stereoselective azirdination (18, 25) and from C–H bond amination reactivity (5–8, 19). Warren and co-workers (6) reported that thermal fragmentation of stable dicopper(II) imido complexes affords a terminal nitrene intermediate through which aliphatic C–H amination occurs. Company and co-workers (22) reported the x-ray absorption near-edge structure (XANES) and extended x-ray absorption structure study of an organic azide reaction with a cuprous precursor, suggesting a Cu(I)/Cu(II) formulation for the reactive intermediate featuring Cu–N bond metrics exceeding those reported by Warren for the dicopper imido complexes. Isolation and solid-state characterization of the nitrenoid adduct is critical to permit a rigorous examination of its molecular structure and disambiguate its electronic configuration. The terminal [Cu(NR)] fragment could exist in a number of electronic formulations, including a high-valent copper imido [Cu(III)(NR)] (Fig. 1A), an iminyl adduct in which Cu is not fully oxidized and N is suboctet [Cu(II)(^{2}NR)] (Fig. 1B), or a nitrene adduct of copper in which the Cu functions as a simple Lewis acid to which the subvalent N moiety is bound [Cu(I)(^{1}NR/^{3}NR)] (Fig. 1C) (26). Whereas metal-ligated imido and iminyl complexes have been isolated and spectroscopically characterized, examples of metal-supported nitrene adducts have thus far eluded full characterization. The electronic structure of the putative [Cu(NR)] fragment is of fundamental interest not only to assess the valence states of the Cu–N pair but also to understand how the [Cu(NR)] electronic structure facilitates nitrene-transfer reaction chemistry. Furthermore, understanding the electronic structure of these critical intermediates is paramount to designing robust catalysts for heteroatom incorporation into unactivated C–H bonds. Here, we report the isolation and characterization of a terminal copper nitrene adduct, assess its electronic structure and Cu/N oxidation states, and describe its attendant amination reaction chemistry.

Metal-ligand multiple bonds (MLMBs) can be highly reactive intermediates through which heteroatom functionality is transferred to unreactive substrates (e.g., C–H bond functionalization). The reactivity of the MLMBs of the 3d elements can be divided into early, mid-, and late 3d transition metal complex behavior. Early 3d transition metal MLMBs are highly polarized, leading to nucleophilic, dianionic imido ligands and electrophilic metal centers. Early transition metal MLMB can exhibit 1,2 addition across the multiple bond as a result of this polarization (27). Progressing across the 3d period, the transition metal valence orbital energies more closely approximate the main group element energies, giving rise to more covalent MLMB interactions (Fig. 1B). The reactivity profiles of MLMBs on mid-3d transition metals are highly sensitive to electronic structure. Whereas low-spin electronic configurations enforce stability (23), open-shell configurations substantially enhance reactivity for group transfer catalysis (28–31). Indeed, biological hydroxylation mediated by cytochrome P450 relies on iron-oxo units partially destabilized by the electron population of Fe–O π^* orbitals (32). Although late-3d transition metal MLMBs have been invoked in a variety of group transfer catalytic processes, MLMBs beyond iron are exceedingly rare,

although demonstrated, for Co (24, 29, 33–35) and Ni (36, 37). Late-3d transition metals feature high d electron counts while simultaneously displaying poor spatial and energetic overlap, wherein inversion of the transition metal and ligand valence orbital energies is possible (Fig. 1C). In an inverted ligand field configuration, the frontier molecular orbitals (MOs) are dominated by ligand character, leaving the metal in a more reduced state (38, 39). Thus, although the bond order will not be altered, the true oxidation levels of the Cu-ligand pair (i.e., Cu(I) d^{10} versus Cu(III) d^8) are impacted and can only be resolved by full x-ray absorption analysis. The subvalent nitrene may correlate with higher electrophilicity and give rise to greater reactivity.

In targeting a terminal copper-nitrenoid complex, we sought to incorporate abundant steric protection as a means of preventing dimerization (6, 9, 17, 19) or nitrene expulsion (40). Accordingly, we selected a dipyrrin scaffold with sterically encumbered peralkylated hydridacene EMind substituents (EMind: 1,1,7,7-tetraethyl-1,2,3,5,6,7-hexahydro-3,3,5,5-tetramethyl-s-indacene) (41, 42). The 2-EMind-1*H*-pyrrole was prepared on multi-gram scales (68% isolated yield) by a modified Negishi protocol (available in the supplementary materials), constituting an unusual example of $C(sp^2)$–$C(sp^2)$ bond formation with ortho/ortho′ quaternary carbons. Acid-catalyzed condensation with 3,5-bis(trifluoromethyl)aldehyde (1,2-dichloroethane; 110°C; 72 hours) provided the corresponding dipyrromethane, which was subjected to oxidation with 2,3-dichloro-5,6-dicyano-1,4-benzoquinone to afford the resulting dipyrrin (^{EMind}L)H in 75% isolated yield after bulk recrystallization from isopropanol/hexanes on multi-gram scales.

Under an atmosphere of nitrogen, treatment of (^{EMind}L)H in benzene with mesitylcopper (1.2 equivalents) for 72 hours at 95°C led to the formation of a single diamagnetic species, as ascertained by ^{1}H and ^{19}F nuclear magnetic resonance (NMR) spectroscopy. Single-crystal x-ray diffraction revealed the corresponding product to be (^{EMind}L)Cu(N_2) (1) (Fig. 2B). The geometry around the metal center is rigorously planar, with the EMind substituents positioned almost orthogonal to the dipyrrin plane [88.1(3)°, 85.7(3)°]. The short N–N bond length [1.085(4) Å] and N–N stretching frequency ($\nu^{14}{}_{N2}$ = 2242 cm^{-1}, $\nu^{14}{}_{N2}$ = 2167 cm^{-1}) indicated minimal activation through back **π**–electron donation from Cu (fig. S59). Indeed, the stretching frequency obtained for **1** represents the least activated molecular dinitrogen adduct thus reported (43, 44) and is comparable to those observed in the impregnated zeolite Cu-ZSM-5 (2295, 2007 cm^{-1}; ZSM: Zeolite Socony Mobil) (45). Although bridging dinitrogen adducts of higher nuclearity on Cu are known (46, 47), **1** represents a rare terminal dinitrogen adduct for Cu or any coinage metal. Displacement of N_2 was apparent by effervescence on exposure to Lewis bases such as pyridine or azides (see below).

Structural characterization of isolated copper nitrenes

With gram quantities of crystalline **1** accessible, nitrene installation from aryl azides was targeted (Fig. 2A). The addition of a C_6D_6 solution of 3,5-bis(methoxy)phenyl azide to solid **1** (0.1 mmol) in silanized glassware led to immediate effervescence along with a color change of the reaction solution from translucent orange to deep orange-red. Monitoring the reaction progress by ^{19}F NMR spectroscopy revealed rapid consumption of starting material

and formation of a major diamagnetic intermediate, a presumed azide adduct [i.e., (^{EMind}L)Cu(N_3Ar)], and a minor, broad paramagnetically shifted resonance, which became the sole resonance over several hours, accompanying a color change to dark red. Single-crystal x-ray diffraction on crystals grown from slow evaporation of pentane solution of the reaction product revealed the bimolecular C–C coupled species [(^{EMind}L)Cu]$_2${N[3,5-(MeO)$_2$C$_6$H$_3$]$_2$}$_2$ (**2**) (Fig. 2C). Exceptionally short Cu–N_{Ar} bond lengths [1.769(4), 1.758(4) Å] and dearomatization of the nitrene aryl moieties [benzene C–C_{avg}: ~1.39 Å; 2: C_{ipso}–C_{ortho}: 1.454(5), 1.450(6), 1.479(6), 1.468(6) Å] are indicative of diketimide formation in 2, similar to previously reported analogous species arising from aryl C–C radical coupling (7). The perpendicular-mode electron paramagnetic resonance (EPR) spectrum of 2 in 2-methyltetrahydrofuran at 10 K is consistent with two uncoupled radicals (fig. S13). The formation of the bridging C–C bond [1.594(6) Å] is reversible by treatment of isolated **2** with trimethylphosphine in C_6D_6 to produce (^{EMind}L)Cu(PMe_3) and the corresponding iminophosphine Me_3PNAr in equal quantities, as ascertained by ^{31}P NMR spectroscopy.

To prevent the radical coupling reaction re sponsible for **2**, we canvassed the reactivity of **1** with para-substituted aryl azides. For example, the addition of a C_6D_6 solution of 4–(^{t}BuO)$C_6H_4N_3$ or 4–(^{t}Bu)$C_6H_4N_3$ to solid **1** resulted in immediate effervescence along with the emergence of two ^{19}F NMR resonances with perturbed aryl azide stretching frequencies by infrared spectroscopy, supporting intermittency of an aryl azide adduct (syntheses of **3** and **4** are provided in the supplementary materials). The diamagnetic (^{EMind}L)Cu(N_3Ar) species was consumed over several hours, as ascertained by ^{1}H and ^{19}F NMR spectroscopy (figs. S62 and S63), leaving only the paramagnetically shifted ^{1}H NMR resonances and a single ^{19}F NMR resonance (Fig. 3E and fig. S17). Near-identical paramagnetic ^{1}H NMR resonances were observed for a library of para-substituted aryl azides, suggesting similar molecular connectivity in different crude reaction mixtures (fig. S64). The paramagnetically shifted resonances were assigned as dipyrrin and arene substituent signals on the basis of azide deuteration experiments and a comparison of aryl azide added to the related dipyrrin(copper) synthon (^{Ar}L)Cu [^{Ar}L: 5-mesityl-1,9-(2,4,6-$Ph_3C_6H_2$)dipyrrin] (48) (figs. S66 and S67). ^{1}H NMR resonances of the reaction products derived from electron-rich aryl azides persisted in perdeuterated benzene for several days at room temperature. Single crystals obtained from the respective addition of 4–(^{t}BuO)$C_6H_4N_3$ or 4–(^{t}Bu)$C_6H_4N_3$ to 1 [0.1 mmol scale; isolated yields: 89% (**3**) and 92% (**4**)] confirmed the formation of the terminal copper-nitrenoid adducts (^{EMind}L)Cu[N($C_6H_4O^tBu$)] (3) (Fig. 2D) and (^{EMind}L)Cu[N($C_6H_4{}^tBu$)] (**4**) (Fig. 3A). A spacefilling model of **4** (Fig. 3C) illustrates how the rigid EMind methyl motifs flank the Cu–N bond, shielding the (Cu–NAr) unit from deleterious reactivity. Whereas azide addition to the sterically more accessible (^{Ar}L)Cu leads to similar ^{1}H NMR spectroscopic resonances (Fig. 3D), incomplete consumption of (^{Ar}L)Cu was observed before complete thermal degradation of the copper-nitrenoid complexes in hours. The solution-phase magnetic moments [**3**: 2.8(1) μ_B; **4**: 2.9(1) μ_B], featureless perpendicular-mode EPR spectra, and paramagnetically shifted ^{1}H NMR resonances corroborate triplet spin states (expected 2.83 μ_B for S = **1**).

The crystal structures for **3** and **4** exhibit exceptionally short Cu–N_{Ar} bonds [3: 1.745(2) Å; **4**: 1.759(2) Å] and near-linear Cu–N_{Ar}–C_{ipso} angles [**3**: 175.8(2)°; **4**: 174.1(2)°]. Closer inspection of the bond lengths of nitrenoid adducts **3** and **4** revealed the nitrenoid functionalities to be redox non-innocent ligands (49). Both **3** and **4** manifest disruption of the N_{Ar} aromaticity: each feature contracted N_{Ar}–C_{ipso} bonds [**3**: 1.321(3) Å; **4**: 1.310(3) Å], elongated C_{ipso}–C_{ortho} bonds [**3**: 1.428 (4), 1.419(**4**) Å; 4: 1.431(3), 1.437(3) Å], contracted C_{ortho}–C_{meta} bonds [3: 1.378(4), 1.373(4) Å; **4**: 1.377 (3), 1.369(3) Å], and elongated C_{meta}–C_{para} bonds [3: 1.404(4), 1.393(4) Å; 4: 1.411(3), 1.402(3) Å] in accord with persistent radical delocalization (Fig. 3B). Similar structural distortions were observed in previously reported iron aryl iminyl complexes (31, 50). The Cu–$N_{dipyrrin}$ bond lengths [**3**: 1.944 (2), 1.942(2) Å; **4**: 1.944(2), 1.940(2) Å] are comparable to those of the unambiguous cuprous **1** [1.942(2), 1.937(2) Å] and substantially longer than the corresponding Cu–$N_{dipyrrin}$ bond in related dipyrrin cupric complexes [e.g., (^{EMind}L)CuCl (**8**), 1.901(3), 1.894(3) Å], potentially signifying a cuprous state rather than a higher Cu oxidation state.

Evidence for a Cu(I) configuration

On the basis of the paramagnetically shifted ^{1}H NMR spectra, the Cu–N linkages in **3** and **4** could represent nitrene adducts of copper [i.e., Cu(I)(^{3}NR)], iminyl adducts [i.e., Cu(II) (^{2}NR)], or high-valent copper imido complexes [i.e., Cu(III) (NR)]. To more precisely ascertain the oxidation states of the copper and nitrogen centers in these complexes, we performed multinuclear x-ray absorption spectroscopy (XAS), interrogating the Cu K-edge, Cu $L_{2,3}$-edge, and N K-edge features of **4**. To assist in the analysis, three-coordinate cuprous and cupric reference complexes featuring only nitrogen-based ligands in the primary coordination sphere were synthesized. An unambiguous Cu(I) complex (^{EMind}L)Cu[$H_2N(C_6H_4{}^tBu)$] (**5**) was prepared by addition of the corresponding aniline to **1** [Cu–$N_{aniline}$: 2.018(6) Å; Cu–$N_{dipyrrin}$: 2.010(6), 2.034(5) Å; Cu–$N_{aniline}$–C_{ipso}: 125.2(5)°]. The Cu(II) anilido (^{EMind}L)Cu[$HN(3,5\text{-}(CF_3)_2C_6H_3)$] [**7**; Cu–$N_{anilido}$: 1.825(2) Å; Cu–$N_{dipyrrin}$: 1.932(2), 1.929(2) Å; Cu–$N_{aniline}$–C_{ipso}: 135.2(2)°] was prepared by oxidation of **1** with excess di-*tert*-butyl peroxide (3.0 equivalent; 60°C; 14 hours) to afford (^{EMind}L)Cu(O^tBu) (**6**), followed by proto-metalation with 3,5-bis(trifluoromethyl)aniline with concomitant release of *tert*-butanol.

The Cu K-edge spectrum featuresa rising edge energy for **4** (8995.7 eV) at higher energy relative to Cu(I) (**5**, 8992.1 eV) and Cu(II) (**7**, 8995.0 eV) (Fig. 4A and fig. S75). A small pre-edge absorption is observed in the experimental spectra of both **4** (8980.0 eV) and **7** (8979.0 eV) (Fig. 3A, inset). A pre-edge shoulder is also partially resolved in the spectrum of **5** at 8980.6 eV. To facilitate assignment of the Cu K pre-edge features, time-dependent density functional theory (TDDFT) calculations were performed for species **4**, **5**, and **7**. Small pre-edge features were predicted for species 5 (8980.4 eV) and 7 (8978.7 eV) and assigned as excitations to ligand-dominated MOs (figs. S71 to S75) (51). Agreement between experimental and TDDFT-calculated Cu K-edge XANES for **4** is weaker than for the other species, but this is attributable to the multiconfigurational nature of the ground state of **4** (see below). Cu K-edge XANES is problematic to rely on for unambiguous assignments of Cu physical oxidation states in formally high-valent systems (39, 52).

Turning to Cu $L_{2,3}$-edge XAS (Fig. 4B), the L_3 mainline features (formally Cu $2p_{3/2} \rightarrow 3d$ transitions) occur at 931 eV (**4**) with an intensity that is severely diminished compared with **7** (930.5 eV). The L_3 intensity of **4** more closely resembles that of **5** (931.2 eV). Experimental estimations of the Cu 3d character in the acceptor orbitals of **4** (14 ± 1.1%) and **7** (53 ± 3.2%) by using methods previously described by Cramer, Solomon, and co-workers (53) are in accord with calculations (**4**: 13.7%; **7**: 52.8%) (table S1). The substantial attenuation of Cu 3d character in **4** juxtaposed with **7** supports a low-valent cuprous assignment with the majority of hole character contained in N-localized orbitals. Our assignment is further supported by N K-edge XAS data and TDDFT calculations that reveal two low-energy pre-edge features at 395.25 eV and 395.85 eV for **4** with substantially more intensity than that observed for **7** at 396.55 eV (Fig. 4C) (54). This splitting and intensity are well reproduced by TDDFT calculations (carried out by using crystallographic coordinates and the B3LYP hybrid density functional) of the N K-edge (fig. S77) (55, 56). A spectroscopy-oriented configuration interaction (SORCI) (57) calculation based on a complete active space (CAS) (12,8) reference was carried out by using a truncated model of **4** with H-atom positions optimized by using the BP86 density functional (58, 59). This calculation indicates that the ground-state triplet is multiconfigurational (fig. S93). The Cu(I)-triplet nitrene configuration (CFG) dominates (58%, CFG 1; Fig. 5) wherein the nitrene coordinates to Cu by means of a dative donation of a lone pair, and the unpaired electrons reside in the N $2p_x$ (MO 139) conjugated to the nitrene aryl and the N $2p_y$ (MO 140). The next most substantial configuration contribution [ferromagnetic coupling of Cu(II)–^{2}NR, CFG 2; Fig. 5], which accounts for only 25% of the ground state, involves charge transfer from Cu to N, leaving the Cu $3d_{xy}$ (MO 135) and N $2p_x$ (MO 139) partially occupied. The remaining configurations in the ground state have very low weights. The largest two of these are Cu(III)–imido (2.7%) and a distinct ferromagnetic Cu(II)–iminyl (1.3%) configurations; the remaining configurations each account for less than 1% of the ground state.

The electronic structure presented from XAS and multireference computations corroborates a cuprous triplet aryl nitrene formulation [i.e., Cu(I)(^{3}NAr)]. One nitrene radical (N $2p_x$) is stabilized by delocalization into the nitrene aromatic ring, whereas the second N $2p_y$ radical is primarily confined to N. There are nonzero (12.3 and 19.0%) contributions of Cu 3d into both of the redox-active orbitals (Fig. 5), which may give rise to the linear Cu–N_{Ar} geometry observed. Orienting the N $2p_y$ with the Cu $3d_{xy}$ orbital (highest in energy from Cu–$N_{dipyrrin}$ σ^*) provides some stabilization of the N $2p_y$ radical, leaving the N $2p_x$ radical to delocalize in the nitrene aryl moiety. The calculated Löwdin (60) bond order (1.21) for the [Cu(NAr)] unit and enhanced N–C_{ipso} bond order (1.50) are consistent with a formulation indicative of minimal metal-ligand multiple bonding. The asymmetry in the N K-edge pre-edge features is reflected in the SORCI degree of N contribution to each state in which the N $2p_x$ contribution is diminished because of delocalization into the arene π system. Free aryl nitrenes display triplet configurations yet typically act as one-or two-electron oxidants when bound to a transition metal center (61). Yet, the electrophilic copper centers in **3** and **4** stabilize the nitrene adducts, preserving their triplet configurations. Remarkably, the Cu center in **4**, and by extension **3**, is best described as Cu(I) as opposed to higher-valent alternatives [i.e., Cu(II) and Cu(III)]. The higher-valent alternatives would require

substantive Cu–N π bonding, which is minimal in nitrene adducts **3** and **4** despite the short $Cu–N_{Ar}$ bond distances observed. The lack of Cu–N π bonding is consistent with the minimal activation of molecular nitrogen in the N_2 adduct **1**. The inverted ligand field observed for nitrene adducts **3** and **4** indicates that the Cu valence orbitals are lower in energy than the corresponding nitrene N *2*p valence orbitals, leaving the redox-active MOs as primarily N based (Fig. 1C).

Nitrene reactivity

To establish the kinetic competency of nitrene adducts in Cu-mediated amination and aziridination, we canvassed the reactivity profile of **4** for nitrene transfer, activation/atom abstraction, and C–H amination. Complete nitrene-transfer reactivity was observed on treatment of **4** with trimethylphosphine to yield phosphinimide and the corresponding copper-ligated phosphine adduct (^{EMind}L)Cu(PMe_3) (fig. S52). Treatment of **4** with the strong nucleophile *tert*-butyl isocyanide (CN^tBu) affordeda rapid color change on mixing from red-orange to orange, generating (^{EMind}L)Cu(CN^tBu) and the corresponding azoarene, as validated by ^1H and ^{19}F NMR spectroscopy as well as independent synthesis (fig. S55). Although nitrene expulsion after intermittent CN^tBu ligation to afford azoarene is favored on the basis of the steric profile, an intermolecular coupling pathway cannot be excluded (fig. S56). Complex **4** was competent for aromatization of 1,4-cyclohexadiene to afford the aniline adduct **5**, demo strating viability for C–H activation. Dissolution of **4** in toluene afforded no changes in ^1H NMR resonances, indicating incapacity to activate benzylic C–H bonds at room temperature. Background decomposition of 4 under mild heating (40°C) was prevalent, suggesting that a more electron-deficient nitrene motif might be required to activate strong C–Hbonds undermild conditions.

Attenuating the steric profile of the supporting dipyrrin ligand and employing electron-deficient aryl azides afforded productive C–H bond amination reactivity. Treatment of thawing solutions of (^{Ar}L)Cu with a stoichiometric electron-poor aryl azide [i.e., 3,5-$(CF_3)_2C_6H_3N_3$, 4-$(CF_3)C_6F_4N_3$, or $C_6F_5N_3$] furnished the corresponding C–H amination products for cyclohexene (77%, 43%, 24%), toluene (71%, 58%, 45%), and cyclohexane (14%, 30%, 36%) in neat substrate, respectively (Fig. 6). Treatment of (^{Ar}L)Cu with 3,5-$(CF_3)_2C_6H_3N_3$ in neat thawing C_6D_6 afforded transient paramagnetic resonances akin to those of **3** and **4** as well as the product of **1** reacting with 3,5-$(CF_3)_2C_6H_3N_3$, suggesting formation of an analogous intermediate copper-nitrenoid species (fig. S67). The reaction of (^{Ar}L)Cu with 3,5-$(CF_3)_2C_6H_3N_3$ in cyclohexene could be rendered catalytic [10 mol % (Cu), 53% yield]. Stark differences in reaction kinetics were observed: Whereas complete consumption of 3,5-$(CF_3)_2C_6H_3N_3$ occurred over extended time frames (~12 hours), consumption of 4-$(CF_3)C_6F_4N_3$ was substantially faster (~4 hours), with $C_6F_5N_3$ requiring the shortest time (~0.5 hours). Aziridination of styrene (5 equivalents in C_6D_6) from (^{Ar}L)Cu was similarly observed (28%, 71%, 86%), albeit over longer time scales (~12 hours) and with mild heating (40°C) for 3,5-$(CF_3)_2C_6H_3N_3$ because of competing coordination of styrene versus aryl azides to (^{Ar}L)Cu. Although only the C–N functionalized product was observed by ^{19}F NMR for toluene amination or styrene azirdination with 4-$(CF_3)C_6F_4N_3$ or $C_6F_5N_3$, EPR analysis on crude reaction mixture confirmed the formation of the corresponding Cu(II) anilido as the major byproduct (figs. S68 and S69). The Cu(II)

anilides (^{Ar}L)Cu[HN(3,5-$(CF_3)_2C_6H_3$)] (**9**) and (^{Ar}L)Cu [HN(C_6F_5)] (**10**) were independently prepared by treatment of (^{Ar}L)CuCl with the corresponding lithium anilide in thawing benzene. Complex **9** and **10** were competent for aromatization of 1,4-cyclohexadiene and radical recombination with either $Ph_3C(C_6H_5)CPh_2$ or alkyl radicals generated in situ with di-*tert*-butyl peroxide, illustrating bona fide radical character on the nitrogen motif, fully consistent with the N K-edge spectrum of **7**. Nonetheless, dissolution of **9** or **10** in toluene afforded no consumption of starting material, suggesting neither **9** nor **10** is not competent for the activation of stronger C–H bonds. These results demonstrate the capacity of copper nitrene species for C–H amination and C–H aziridination.

Outlook

The foregoing data demonstrate the role of a sterically encumbered ligand scaffold to support a thermally robust copper-ligated triplet aryl nitrene. The isolation, structural determination, and spectroscopic interrogation of the nitrene adducts allow us to clearly determine both the Cu and N valence states. A priori, redox formalisms would suggest that the Cu centers should exhibit higher oxidation states [e.g., Cu(II)(^{2}NR) or Cu(III)(NR)], achieving a filled octet at the more electronegative N center. The short Cu–N bond distances observed by crystallography for the nitrene adducts suggest Cu–N π bonding consistent with that formulation. However, the x-ray absorption data reveal a more nuanced picture wherein the Cu site maintains a mono-valent state and the nitrene resides in a subvalent state, dominating the redox-active frontier MOs. The electronic configuration is in accord with the increasing body of literature that nominally high-valent copper ions are subject to an inverted ligand field with minimal physical oxidation on the copper center (38, 39, 62, 63). The conclusions presented herein should facilitate a refined consideration of how the presence or absence of MLMBs in late–transition metal complexes influence group transfer catalysis.

Supplementary Material

Refer to Web version on PubMed Central for supplementary material.

ACKNOWLEDGMENTS

We thank R. Y. Liu and S. L. Buchwald (MIT) for helpful discussions on the construction of 2-EMind-1*H*-pyrrole. We thank M. Nava and Y. Jing (Harvard) for assistance in the infrared spectrum measurement of $^{15}N_2$-labeled

1. Funding: T.A.B. acknowledges a grant from the NIH (GM-115815), the Dreyfus Foundation (Teacher-Scholar Award), and Harvard University. K.M.C. acknowledges the Fannie and John Hertz Foundation and the National Science Foundation for financial support of this research. K.M.L. acknowledges NSF (CHE-1454455) and the Alfred P. Sloan Foundation for financial support. XAS data were obtained at SSRL, which is supported by the U.S. Department of Energy Office of Science and Office of Basic Energy Sciences (contract no. DE-AC02–76SF00515). The SSRL Structural Molecular Biology Program is supported by the Department of Energy's Office of Biological and Environmental Research and NIH/HIGMS (including P41GM103393). The work at SSRL was also supported by the U.S. Department of Energy Office of Basic Energy Sciences (proposal no. 100487).

REFERENCES AND NOTES

1. Zalatan DN, Bois JD, in C-H Activation, Yu J-Q, Shi Z, Eds. (Springer Berlin Heidelberg, 2010), pp. 347–378.

2. Gephart III RT, Warren TH, Organometallics 31, 7728–7752 (2012).
3. Chemler SR, Science 341, 624–626 (2013). [PubMed: 23929974]
4. Kwart H, Khan AA, J. Am. Chem. Soc 89, 1951–1953 (1967).
5. Díaz-Requejo MM, Belderraín TR, Nicasio MC, Trofimenko S, Pérez PJ, J. Am. Chem. Soc 125, 12078–12079 (2003).
6. Badiei YM et al., Angew. Chem. Int. Ed 47, 9961–9964 (2008).
7. Bakhoda AG, Jiang Q, Bertke JA, Cundari TR, Warren TH, Angew. Chem. Int. Ed 56, 6426–6430 (2017).
8. Bakhoda A. et al., Angew. Chem. Int. Ed 131, 3459–3463 (2019).
9. Hamilton CW, Laitar DS, Sadighi JP, Chem. Commun 2004, 1628–1629 (2004).
10. Lv Y. et al., Chem. Commun 49, 6439–6441 (2013).
11. Evans DA, Faul MM, Bilodeau MT, Anderson BA, Barnes DM, J. Am. Chem. Soc 115, 5328–5329 (1993).
12. Li Z, Conser KR, Jacobsen EN, J. Am. Chem. Soc 115, 5326–5327 (1993).
13. Tian X, Hudlicky T, Koenigsberger K, J. Am. Chem. Soc 117, 3643–3644 (1995).
14. Overman LE, Tomasi AL, J. Am. Chem. Soc 120, 4039–4040 (1998).
15. White RD, Keaney GF, Slown CD, Wood JL, Org. Lett 6, 1123–1126 (2004). [PubMed: 15040738]
16. Trost BM, Dong G, J. Am. Chem. Soc 128, 6054–6055 (2006). [PubMed: 16669672]
17. Badiei YM, Krishnaswamy A, Melzer MM, Warren TH, J. Am. Chem. Soc 128, 15056–15057 (2006).
18. Li Z, Quan RW, Jacobsen EN, J. Am. Chem. Soc 117, 5889–5890 (1995).
19. Aguila MJB, Badiei YM, Warren TH, J. Am. Chem. Soc 135, 9399–9406 (2013). [PubMed: 23656170]
20. Kundu S. et al., J. Am. Chem. Soc 134, 14710–14713 (2012).
21. Dielmann F, Andrada DM, Frenking G, Bertrand G, J. Am. Chem. Soc 136, 3800–3802 (2014). [PubMed: 24559041]
22. Corona T. et al., Angew. Chem. Int. Ed 55, 14005–14008 (2016).
23. Nugent WA, Mayer JM, Metal-Ligand Multiple Bonds: The Chemistry of Transition Metal Complexes Containing Oxo, Nitrido, Imido, Alkylidene, or Alkylidyne Ligands (Wiley Interscience, 1988).
24. Berry JF, Comments Inorg. Chem 30, 28–66 (2009).
25. Evans DA, Faul MM, Bilodeau MT, J. Org. Chem 56, 6744–6746 (1991).
26. Cundari TR, Dinescu A, Kazi AB, Inorg. Chem 47, 10067–10072 (2008).
27. Mindiola DJ, Acc. Chem. Res 39, 813–821 (2006). [PubMed: 17115721]
28. Wilding MJT et al., J. Am. Chem. Soc 139, 14757–14766 (2017).
29. King ER, Sazama GT, Betley TA, J. Am. Chem. Soc 134, 17858–71861(2012).
30. Wilding MJT, Iovan DA, Betley TA, J. Am. Chem. Soc 139, 12043–12049 (2017).
31. Iovan DA, Betley TA, J. Am. Chem. Soc 138, 1983–1993 (2016). [PubMed: 26788747]
32. Groves JT, McClusky GA, White RE, Coon MJ, Biochem. Biophys. Res. Commun 81, 154–160 (1978). [PubMed: 656092]
33. Goetz MK, Hill EA, Filatov AS, Anderson JS, J. Am. Chem. Soc 140, 13176–13180 (2018). [PubMed: 30078327]
34. Zhang L, Liu Y, Deng L, J. Am. Chem. Soc 136, 15525–15528 (2014). [PubMed: 25330361]
35. Yao X-N et al., J. Am. Chem. Soc 139, 373–380 (2017). [PubMed: 27936686]
36. Kogut E, Wiencko HL, Zhang L, Cordeau DE, Warren TH, J. Am. Chem. Soc 127, 11248–11249 (2005).
37. Laskowski CA, Miller AJM, Hillhouse GL, Cundari TR, J. Am. Chem. Soc 133, 771–773 (2011). [PubMed: 21175213]
38. Hoffmann R. et al., Chem. Rev 116, 8173–8192 (2016). [PubMed: 27398715]
39. Walroth RC, Lukens JT, MacMillan SN, Finkelstein KD, Lancaster KM, J. Am. Chem. Soc 138, 1922–1931 (2016). [PubMed: 26844693]

40. Takaoka A, Moret M-E, Peters JC, J. Am. Chem. Soc 134, 6695–6706 (2012). [PubMed: 22381423]
41. Matsuo T. et al., Bull. Chem. Soc. Jpn 84, 1178–1191 (2011).
42. Matsuo T, Tamao K, Bull. Chem. Soc. Jpn 88, 1201–1220 (2015).
43. Murray RB, Ferreira LJ, in Transition Metal-Dinitrogen Complexes, Y. Nishibayashi, Ed. (Wiley-VCH Verlag GmbH & Co. KGaA, 2019), pp. 403–439.
44. Holland PL, Dalton Trans. 39, 5415–5425 (2010). [PubMed: 20361098]
45. Itadani A. et al., J. Phys. Chem C 111, 16701–16705 (2007).
46. Murray LJ, Weare WW, Shearer J, Mitchell AD, Abboud KA, J. Am. Chem. Soc 136, 13502–13505 (2014).
47. Zhang S. et al., Angew. Chem. Int. Ed 55, 9927–9931 (2016).
48. Iovan DA et al., Chem. Commun 53, 10306–10309 (2017).
49. Jørgensen CK, Coord. Chem. Rev 1, 164–178 (1966).
50. King ER, Hennessy ET, Betley TA, J. Am. Chem. Soc 133, 4917–4923 (2011). [PubMed: 21405138]
51. Walroth RC, Uebler JWH, Lancaster KM, Chem. Commun 51, 9864–9867 (2015).
52. Tomson NC et al., Chem. Sci 6, 2474–2487 (2015). [PubMed: 29308158]
53. George SJ, Lowery MD, Solomon EI, Cramer SP, J. Am. Chem. Soc 115, 2968–2969 (1993).
54. Lukens JT, DiMucci IM, Kurogi T, Mindiola DJ, Lancaster KM, Chem. Sci 10, 5044–5055 (2019). [PubMed: 31183055]
55. Stephens PJ, Devlin FJ, Chabalowski CF, Frisch MJ, J. Phys. Chem 98, 11623–11627 (1994).
56. Becke AD, J. Chem. Phys 98, 5648–5652 (1993).
57. Neese F, J. Chem. Phys 119, 9428–9443 (2003).
58. Becke AD, Phys. Rev. A Gen. Phys 38, 3098–3100 (1988). [PubMed: 9900728]
59. Perdew JP, Phys. Rev. B Condens. Matter 33, 8822–8824 (1986). [PubMed: 9938299]
60. Löwdin P-O, Phys. Rev 97, 1474–1489 (1955).
61. Olivos Suarez AI, Lyaskovskyy V, Reek JNH, van der Vlugt JI, de Bruin B, Angew. Chem. Int. Ed 52, 12510–12529 (2013).
62. Mankad NP, Antholine WE, Szilagyi RK, Peters JC, J. Am. Chem. Soc 131, 3878–3880 (2009). [PubMed: 19253942]
63. Walroth RC et al., J. Am. Chem. Soc 139, 13507–13517 (2017).

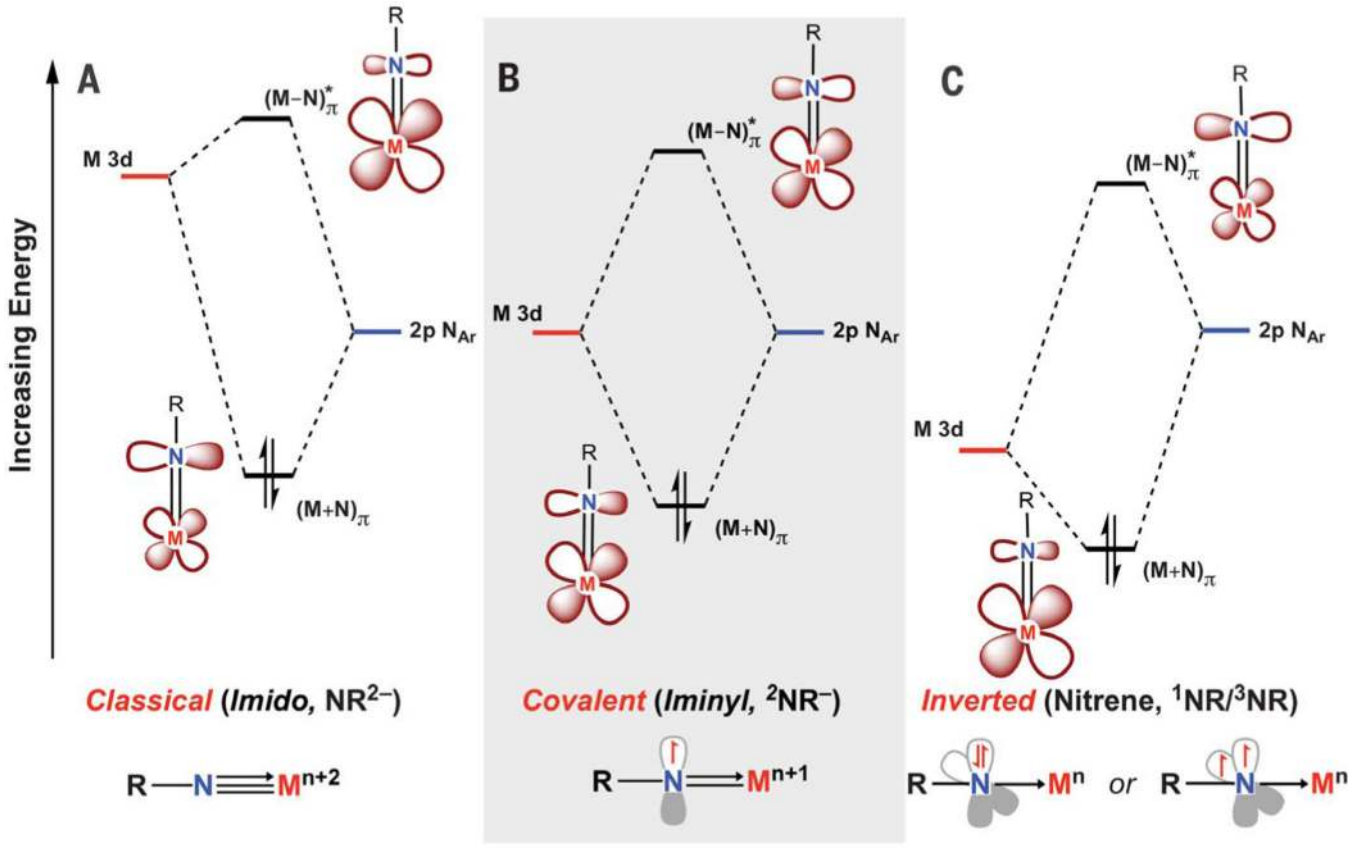

Fig. 1. Oxidation-state formalisms for M(NR) functionality.

(**A**) Metal imido featuring dianionic, closed-shell (NR^{2-}) functional group bound to a doubly oxidized metal. (**B**) Metal-iminyl featuring a monoanionic, open-shell ($^2NR^-$) moiety bound to a singly oxidized metal. (**C**) Singlet or triplet nitrene coordinating a neutral metal.

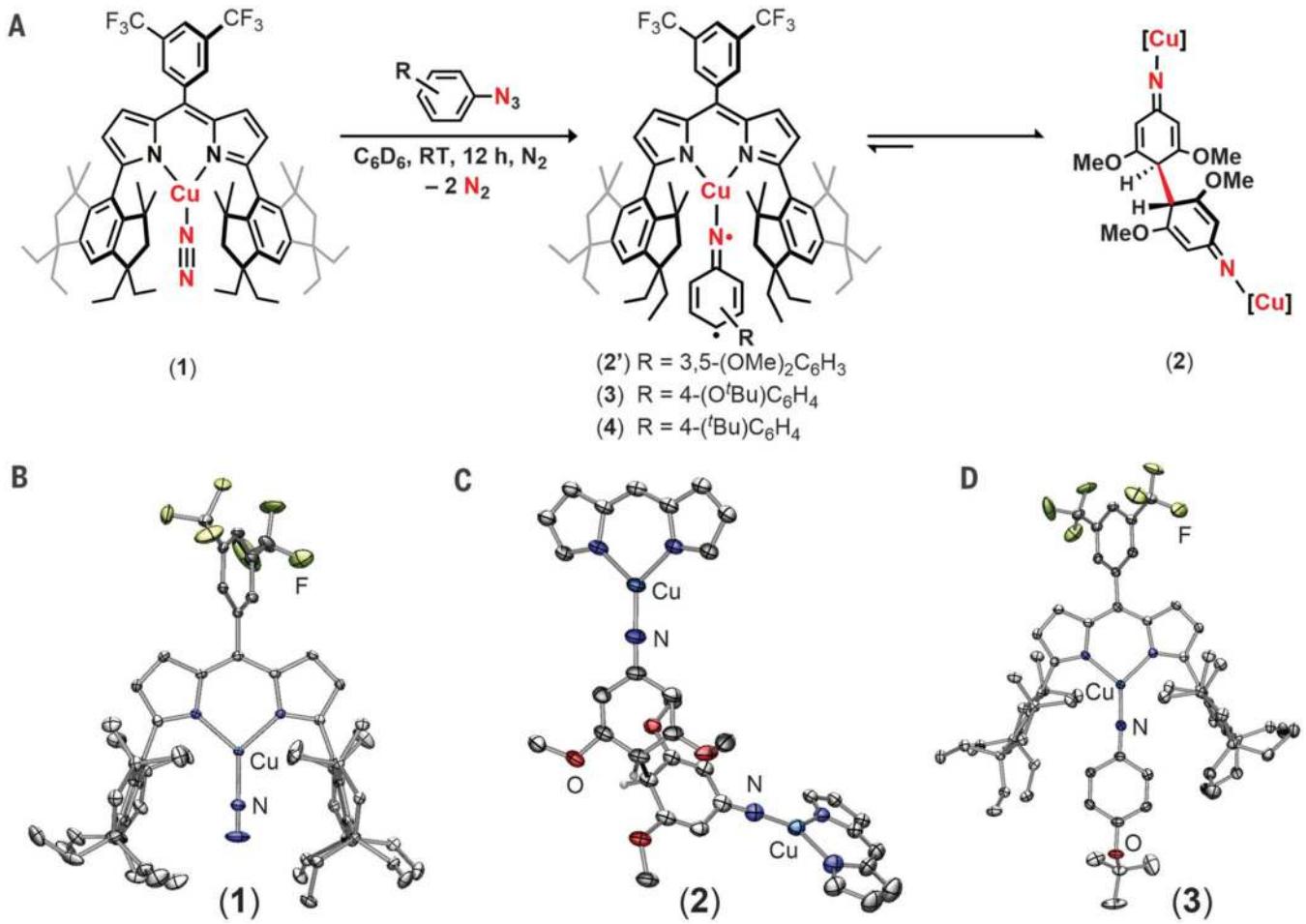

Fig. 2. Copper nitrene preparation and solid-state analysis.

(**A**) Reaction scheme to access terminal (**3** and **4**) and dimeric (**2**) copper-nitrenoid motifs from treatment of (^{EMind}L)Cu(N_2) (**1**) with aryl azides. (**B**) Truncated solid-state structure of **1** at 50% displacement ellipsoid probability. (**C**) Solid-state structure of **2** at 35% displacement ellipsoid probability. (**D**) Solid-state structure of **3** at 50% displacement ellipsoid probability. Color scheme: Cu (cobalt blue), F (yellow-green), N (blue), and O (red).

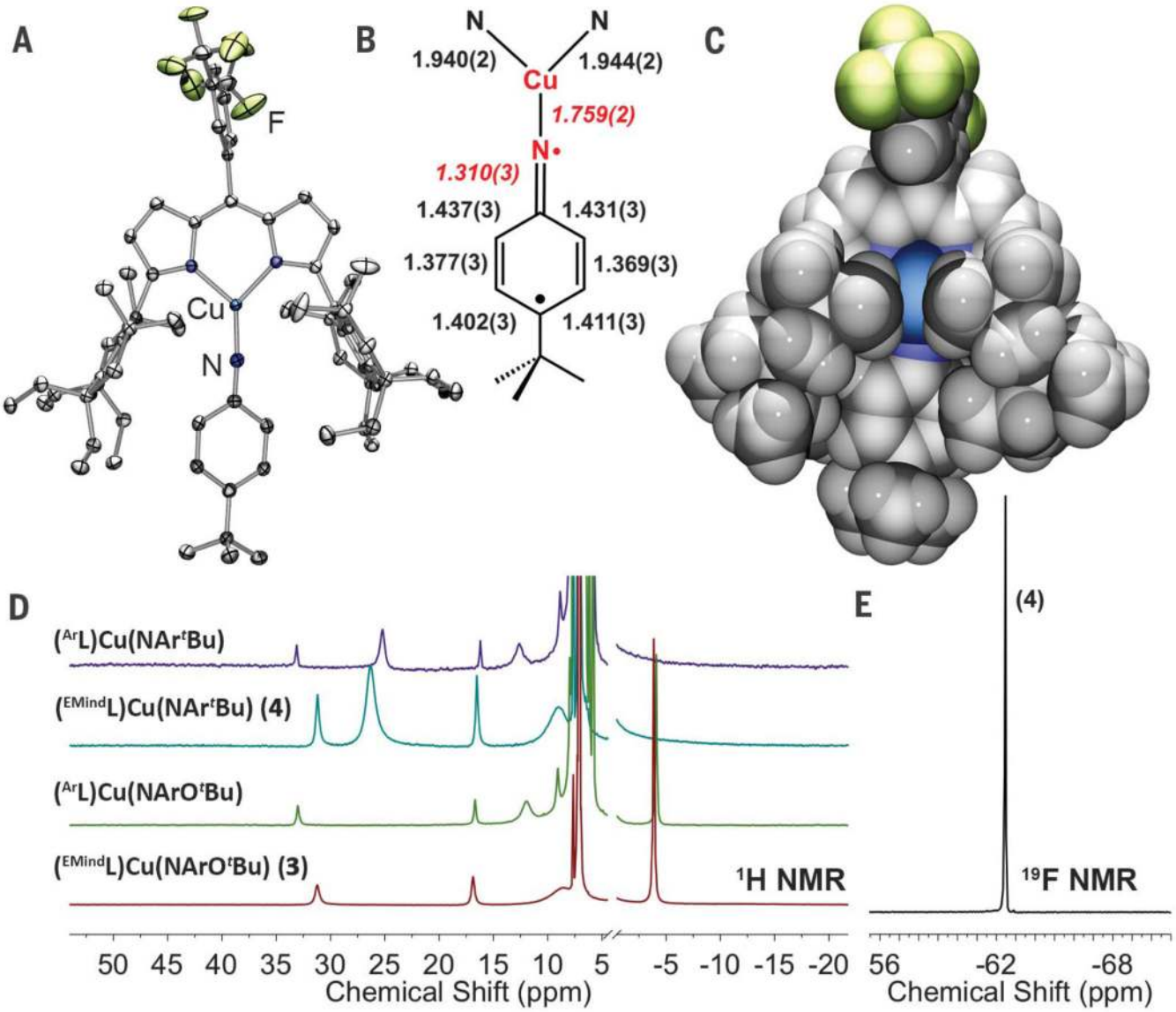

Fig. 3. Copper nitrene isolation and structural analysis.

(**A**) Solid-state structure of (^{EMind}L)Cu[N(C_6H_4*t*Bu)] (**4**) at 50% displacement ellipsoid probability. (**B**) Core bond metrics of {Cu[N(C_6H_4*t*Bu)])} (**4**). (**C**) Space-filling model of **4** depicting steric shielding of the Cu–N bond vector. (**D**) ^{1}H NMR spectrum overlay of (^{EMind}L)Cu[N(C_6H_4O*t*Bu)] (**3**, red), (^{Ar}L)Cu[N(C_6H_4O*t*Bu)] (green), (^{EMind}L)Cu[N(C_6H_4*t*Bu)] (**4**, cyan), (^{Ar}L)Cu[N(C_6H_4*t*Bu)] (purple). (**E**) ^{19}F NMR spectrum of (^{EMind}L)Cu[N(C_6H_4*t*Bu)] (**4**).

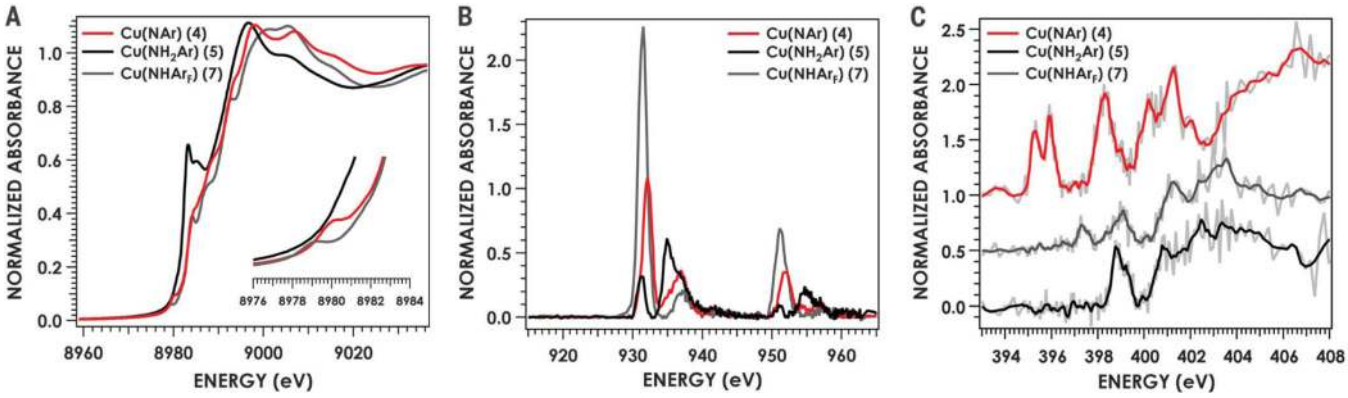

Fig. 4. XAS.

(**A**) Cu K-edge, (**B**) Cu $L_{2,3}$-edge, and (**C**) N K-edge absorption spectra of (^{EMind}L)Cu[N($C_6H_4{}^tBu$)] (**4**, red), (^{EMind}L)Cu[$H_2N(C_6H_4{}^tBu)$] (**5**, black), (^{EMind}L)Cu{HN[3,5-$(CF_3)_2C_6H_3$]} (**7**, gray). Light-gray lines in (C) represent experimental data, with colored lines representing smoothed data.

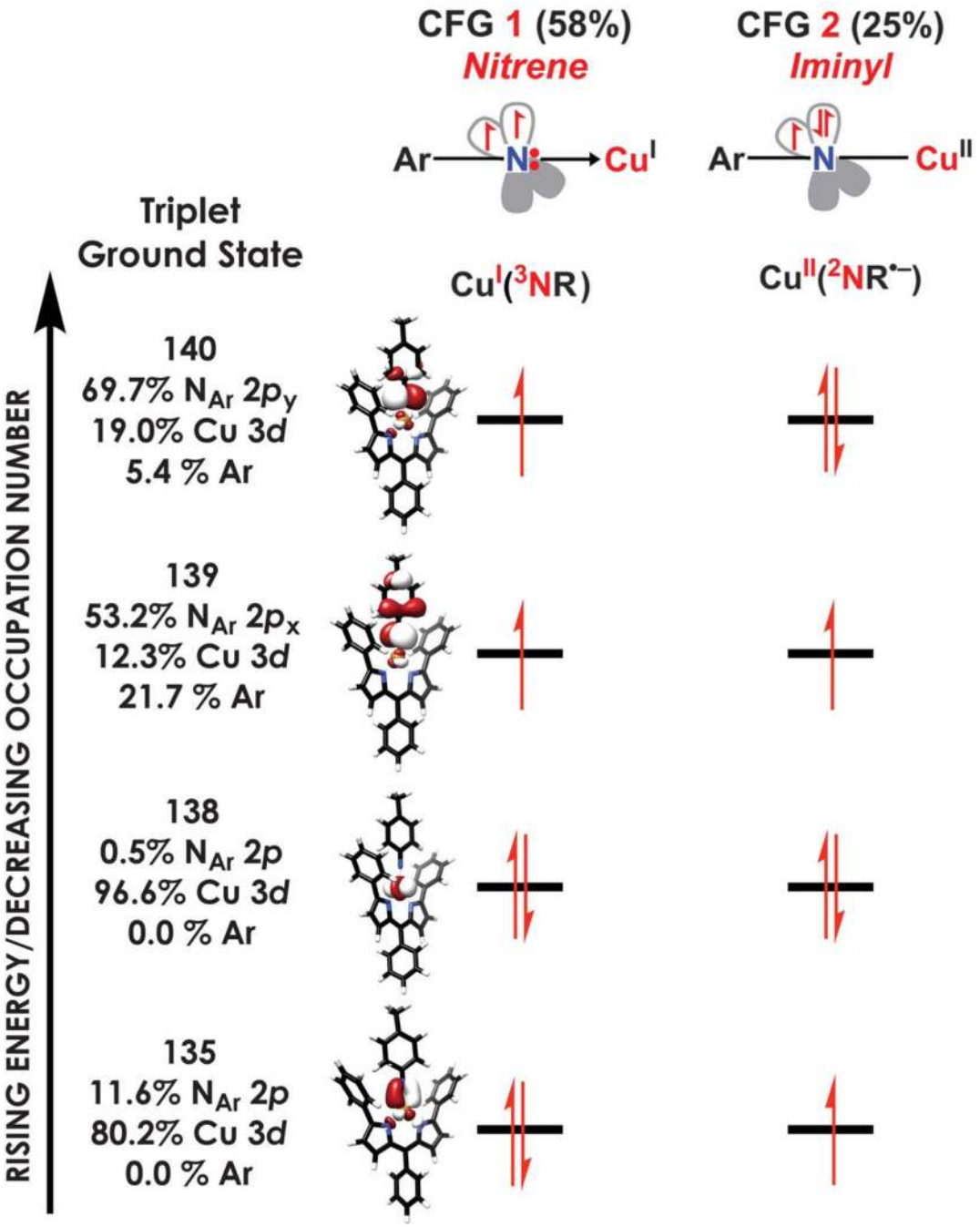

Fig. 5. SORCI calculations.

The 6-electron, 4-orbital subspace of a 12-electron, 8-orbital CAS (12,8) is used to depict leading configurations generated through a SORCI calculation of the triplet ground state of a truncated model of **4**. The dominant configuration (58%) is that of a triplet nitrene bound to a Cu(I) center. The only other significant contribution (25%) has the configuration of a doublet iminyl bound to Cu(II) with the electrons ferromagnetically coupled because of orthogonality of the singly occupied MOs. The remaining configurations in the ground state have very low weights. The largest two of these are Cu(III)–imido (2.7%) and ferromagnetic

Cu(II)–iminyl (1.3%) configurations; the remaining configurations each account for less than 1% of the ground state. Calculations were initiated by using a starting set of orbitals generated through a hybrid density functional theory calculation (B3LYP, ZORA-def2-TZVP(-f) on Cu, N; ZORA-def2-SVP on all other atoms).

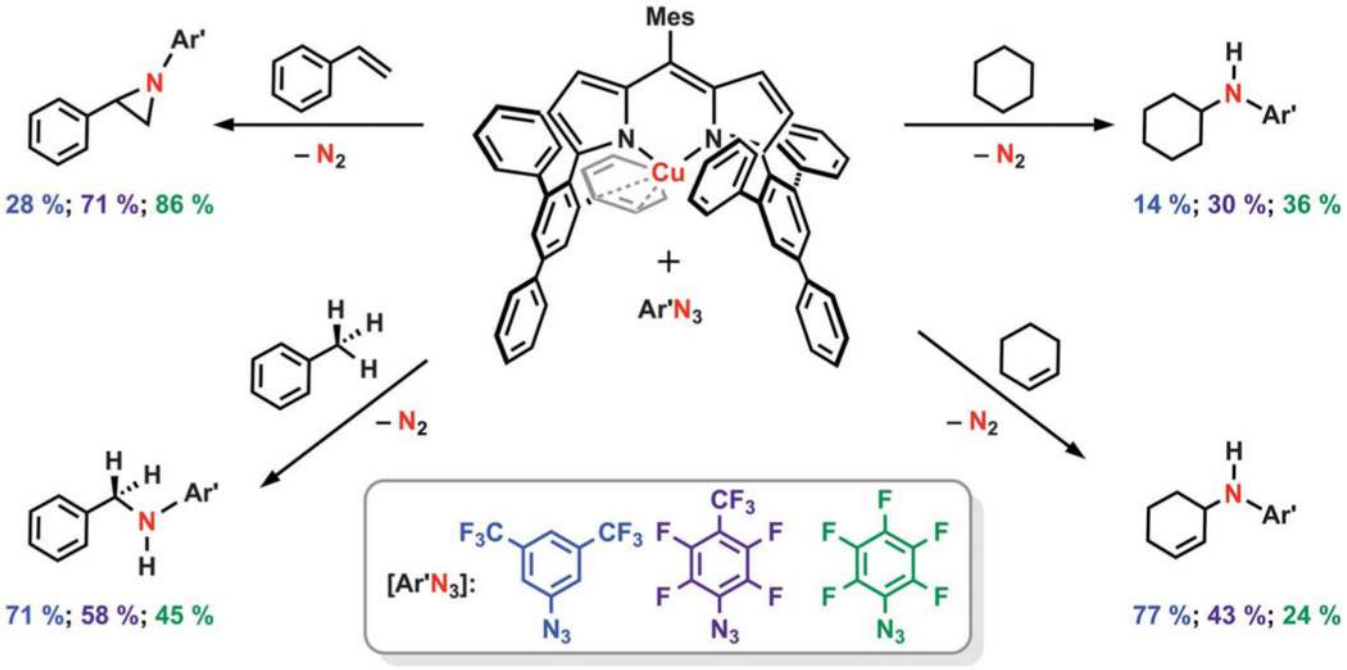

Fig. 6. Nitrene-transfer reactivity.

Treatment of (^{Ar}L)Cu with electron-deficient aryl azides in the presence of substrates affords C–H amination (toluene, cyclohexene, cyclohexane) and azirdination (styrene) products. Yields are reported in triplicate with respect to a ^{19}F NMR internal standard of fluorobenzene.